



PpSCARECROW1 (PpSCR1) regulates leaf blade and mid-vein development in *Physcomitrium patens*

Boominathan Mohanasundaram^{1,2} · Shirsa Palit^{1,4} · Amey J. Bhide¹ · Madhusmita Pala¹ · Kanishka Rajoria¹ · Payal Girigosavi^{1,3} · Anjan K. Banerjee¹

Received: 1 April 2023 / Accepted: 11 December 2023
© The Author(s), under exclusive licence to Springer Nature B.V. 2024

Abstract

In plants, asymmetric cell divisions result in distinct cell fates forming large and small daughter cells, adding to the cellular diversity in an organ. SCARECROW (SCR), a GRAS domain-containing transcription factor controls asymmetric periclinal cell divisions in flowering plants by governing radial patterning of ground tissue in roots and cell proliferation in leaves. Though SCR homologs are present across land plant lineages, the current understanding of their role in cellular patterning and leaf development is mostly limited to flowering plants. Our phylogenetic analysis identified three SCR homologs in moss *Physcomitrium patens*, amongst which *PpSCR1* showed highest expression in gametophores and its promoter activity was prominent at the mid-vein and the flanking leaf blade cells pointing towards its role in leaf development. Notably, out of the three SCR homologs, only the *ppscr1* knock-out lines developed slender leaves with four times narrower leaf blade and three times thicker mid-vein. Detailed histology studies revealed that slender leaf phenotype is either due to the loss of anticlinal cell divisions or failure of periclinal division suppression in the leaf blade. RNA-Seq analyses revealed that genes responsible for cell division and differentiation are expressed differentially in the mutant. *PpSCR1* overexpression lines exhibited significantly wider leaf lamina, further reconfirming the role in leaf development. Together, our data suggests that *PpSCR1* is involved in the leaf blade and mid-vein development of moss and that its role in the regulation of cell division and proliferation is ancient and conserved among flowering plants and mosses.

Key message

The GRAS domain containing protein *PpSCR1* regulates asymmetric cell divisions and governs leaf blade and mid-vein development in moss *Physcomitrium patens*.

Keywords Cell division · GRAS domain · Leaf shape and development · *Physcomitrium patens* · SCARECROW · Slender-leaf

Introduction

Leaf shape has profound influence on light perception, carbon capture and thermoregulation etc., in plants (Takenaka 1994; Nicotra et al. 2011; Leigh et al. 2017; Higuchi and Kawakita 2019; Tamang et al. 2023). Given their critical role, leaves have evolved independently multiple times (Harrison et al. 2005; Tomescu 2009). The large leaves with complex shape and anatomical features, such as megaphylls and microphylls, are present in vascular plants, while bryophytes (non-vascular plants) have phyllids, that are small leaf-like organs with or without a midrib. Megaphylls of flowering plants have been extensively studied and the leaf shape determinants are quite well known. The basis of leaf

✉ Anjan K. Banerjee
akb@iiserpune.ac.in

¹ Indian Institute of Science Education and Research (IISER-Pune), Biology Division, Dr Homi Bhabha Road, Pune 411008, Maharashtra, India

² Currently at Donald Danforth Plant Science Center, St. Louis, MO, USA

³ Currently at National AIDS Research Institute, Pune, Maharashtra, India

⁴ Currently at Cold Spring Harbor Laboratory, Cold Spring Harbor, New York, USA

development has been investigated in moss (Lin et al. 2021; Mohanasundaram et al. 2021; Moody 2022), however, the factors regulating leaf shape have not been explored. The final shape of plant organs is determined by the cell division plane and the rate of cell division and expansion (Gázquez and Beemster 2017; Horiguchi and Tsukaya 2011). Cell division plane attributes, such as the angle and symmetry of division, regulate plant tissue growth. Cells dividing at perpendicular angle (i.e. anticlinal divisions) to the tissue surface increase the number of cells in a tissue layer, whereas cells dividing in parallel (i.e. periclinal divisions) to the tissue surface add to the number of cell layers. Additionally, plant cells frequently make developmental decisions using asymmetric cell divisions (De Smet and Beeckman 2011).

GRAS-domain containing transcription factors, such as SCARECROW (SCR) and SHORTROOT (SHR), regulate cell division plane and organ growth in flowering plants. In Arabidopsis, SCR and SHR modulate radial patterning of the root and the proliferation of leaf cells (Scheres et al. 1995; Dhondt et al. 2010). At the root apical meristem, the cortex endodermal initial cell undergoes an asymmetric division to form the ground tissue comprising the cortex and epidermis. In *scr* mutants, due to the loss of an asymmetric periclinal division, a single layer of ground tissue was formed, having characters of both the cortex and epidermis. In addition, the mutant leaf size was greatly reduced because SCR is required for prolonging the S-phase duration during leaf development (Dhondt et al. 2010). Hence, Scheres et al., (1995) suggested that the SCR transcription factor specifically regulates the asymmetric cell division in Arabidopsis root. Along with SCR, SHR and auxin gradient control the radial patterning and ground tissue development of Arabidopsis roots (Benfey et al. 1993; Clark et al. 2020; Perilli et al. 2012; Scheres et al. 1995).

Among all the bryophytes, leaf-like organs having mid-veins (phyllids) are found only in mosses. The moss gametophores have spirally arranged phyllids (hereafter leaves) on their central axis and rhizoids at the base. These leaves exhibit heteroblasty characters, where the mature leaves are oblanceolate in shape with marginal serrations and a mid-vein, whereas juvenile leaves are Y-shaped and lack mid-veins (Barker and Ashton 2013; Dennis et al. 2019). Moss leaves have uni-layered leaf blade and multi-layered mid-vein. The mid-vein is an unbranched, simple tissue compared to the vasculature found in megaphylls. Interestingly, a common set of transcription factors govern the mid-vein development in mosses and the vasculature formation in flowering plants (Xu et al. 2014; Yip et al. 2016).

Well-orchestrated cell division plane orientation and series of asymmetric divisions at the shoot apex lay the foundation for moss leaf primordium formation. The tetrahedral apical cell of moss gametophore has been shown to divide in three cutting faces, which leads to the formation of leaf

apical cells in a spiral arrangement (Crandall-Stotler and Guerke, 1980). Elegant sector analysis and live imaging of *P. patens* leaves revealed cell division pattern in leaf development (Harrison et al. 2009). The leaf apical cell undergoes a series of asymmetric cell divisions and contributes daughter cells basipetally to form the leaf primordium. The second wave of growth begins from the base of the leaf primordium as each daughter cell initially undergoes two rounds of asymmetric cell divisions along the medio-lateral axis and finally gives rise to a segment of the mature leaf. Though a basic understanding of moss leaf primordia formation exists, further downstream factors controlling leaf shape have not been fully explored.

The homologs of SCR and other GRAS domain containing proteins have been identified in *P. patens* (Engstrom 2011), and their role in asymmetric cell division is being studied (Ge et al. 2022; Ishikawa et al. 2023). Very recently, PpSHR has been shown to govern leaf vein formation in *P. patens* (Ishikawa et al. 2023), and it is positively regulated by PpSCR1, however the study was limited to leaf primordium analysis. Here, we aimed to decipher the molecular and cellular basis of PpSCR1 function in moss leaf development using knockout and overexpression approaches, comparative histology, promoter-reporter analysis and RNA-seq data sets. We demonstrate that out of the three SCR homologs in moss, PpSCR1 regulates asymmetric cell division to influence mid-vein and lamina development.

Materials and methods

Phylogenetic tree construction

To cover the full spectrum of streptophytes, the protein sequences of *Arabidopsis thaliana* (*A. thaliana*), *Oryza sativa*, *Nymphaea colorata*, *Thuja plicata*, *Selaginella moellendorffii*, *Ceratopteris richardii*, *Anthoceros punctatus*, *Physcomitrium patens*, *Sphagnum fallax*, *Marchantia polymorpha*, *Mesotaenium endlicherianum*, *Spirogloea musicola*, *Penium margaritaceum*, *Chara braunii* and *Klebsormidium nitens* were downloaded from Phytozome (<https://phytozome-next.jgi.doe.gov/>) and Phycocosm (<https://phyocosm.jgi.doe.gov/phyocosm>) databases. We retrieved the GRAS domain sequences of *A. thaliana* proteins and constructed HMM (Hidden Markov Model) profile. Using the GRAS domain HMM profile and hmm search tool (<http://hmmer.org/>), homology search was performed to identify the GRAS domain containing proteins across streptophyte genomes. All the sequences were aligned using the multiple sequence alignment software MAFFT version 7.271 (Katoh and Standley 2013), and the gaps were removed using the trimAL program (Capella-Gutiérrez et al. 2009). An initial tree was prepared using RaxML, and duplicate sequences

were removed. The best-fit model was identified using the ModelFinder algorithm, and a maximum likelihood phylogenetic tree was constructed with 1000 bootstrap replicates (Kalyaanamoorthy et al. 2017; Nguyen et al. 2015).

Moss culture and maintenance

Physcomitrium patens ecotype ‘Gransden’ was procured from International Moss Stock Center (IMSC), University of Freiburg, Germany and maintained in vitro (Cove et al. 2009). Homogenized protonemal tissue was grown on cellophane-overlaid BCDAT agar medium. Post homogenization, tissues were incubated for 4–5 days in tissue culture incubators at 16:8 h light: dark cycle at 24 °C for all the experiments. For leaf width assay, seven-day-old protonemal filaments were inoculated in BCD and BCDAT media containing 1 µM 6-Benzylaminopurine (BAP). Leaf width was recorded from the 9th leaf of one-month-old gametophores.

Cloning and plant transformation

The knockout constructs of the three *PpSCR* genes was prepared by cloning the 5′ and 3′ flanking regions into the pTN186 vector (4.5 Kb) (Supplementary Fig S2 and S3). The 5′ and 3′ flanking regions of the three genes were amplified by polymerase chain reaction (PCR) using primer sets (Pp_SCR1_5′_F, Pp_SCR1_5′_R, Pp_SCR1_3′_F, Pp_SCR1_3′_R), (Pp_SCR2_5′_F, Pp_SCR2_5′_R, Pp_SCR2_3′_F, Pp_SCR2_3′_R) and (Pp_SCR3_5′_F, Pp_SCR3_5′_R, Pp_SCR3_3′_F, and Pp_SCR3_3′_R). PCR products were subcloned into pGEM-T vector, and sequence confirmed. PpSCR1 5′ flanking region was cloned into the pTN186 vector between *KpnI* and *Sall* restriction enzyme (RE) sites, and 3′ flanking region was cloned between *SmaI* and *SacI* RE sites. PpSCR2 5′ flanking region was cloned into the pTN186 vector between *KpnI* and *XhoI* RE sites, and 3′ flanking region was cloned between *BamHI* and *NotI* RE sites. PpSCR3 5′ flanking region was cloned into the pTN186 vector between *XhoI* and *HindIII* RE sites, and 3′ flanking region was cloned between *XmaI* and *NotI* RE sites. These constructs were then PCR amplified using the primer pairs Pp_SCR1_5′_F and Pp_SCR1_3′_R, Pp_SCR2_5′_F and Pp_SCR2_3′_R and Pp_SCR3_5′_F and Pp_SCR3_3′_R (Supplementary Table S1) and used for PEG-mediated protoplast transformation. Genomic DNA from *ppscr1* lines was used to confirm the stable lines using the primer pairs of SCR1_KO_5′_fusion_conf F; KO_5′_sGFP_conf R and KO_APH4_conf F; SCR1_KO_5′_fusion_conf R (Supplementary Table S1). Stable *ppscr2* and *ppscr3* lines were confirmed using the primer pairs Sb_Kan qF and Sb_Kan qR and the pair Hyg qF and Hyg qR, respectively. To develop PpSCR1:GUS reporter construct, the *PpSCR1* promoter

(1.9 kb) was amplified from WT genomic DNA using SCR1Prom_XmaI_F and SCR1Prom_XmaI_R primer pairs (Supplementary Table S1). Purified PCR product was cloned into pBI101 vector, and promoter sequence and orientation were confirmed through sequencing. Entire PpSCR1:GUS cassette was amplified using HindIII SCR1Prom F and HindIII_SCR1Prom_NosT R primer pairs and cloned into pCAMBIA1300 vector. For generation of the PpSCR1_OE construct, *PpSCR1* was amplified from WT cDNA using the primer pairs attB1 SCR1 F and attB5r SCR1 R. SCR1-GFP cassette was generated via BP-LR cloning mediated by the entry vectors pENTR 221 (P1P5r) and pENTR L5L2 (containing GFP) and the destination vector pTK-Ubi Gate. The stable lines were confirmed through RT-qPCR with the primer pairs GFP qF; GFP qR and PpSCR1 qF; PpSCR1 qR (Supplementary Table S1).

PEG-mediated protoplast transformation and transgenic line generation

PEG-mediated *P. patens* protoplast transformation was performed as per the protocol of Nishiyama (2000). In brief, seven-day-old protonema was digested with 1% (w/v) driselase mixture (Sigam-Aldrich, Bangalore, India) to release protoplasts and washed with 8% mannitol. Protoplast mixture is then transferred to a 2% PEG solution containing MgCl₂ and Ca(NO₃)₂ and the desired DNA for transformation. DNA uptake by protoplast was facilitated by a heat shock step at 45 °C for five min. The osmolarity of the protoplast solution was brought back using protoplast regeneration media (BCDAT + 6% mannitol + 10 mM CaCl₂) and incubated under darkness for cell wall regeneration. Five days after transformation, regenerated protoplasts were transferred to selection media (BCDAT media containing hygromycin (20 mg/L). After two weeks of incubation, colonies were transferred to BCDAT media for two weeks for relaxation. For secondary selection, colonies were further transferred to BCDAT media containing hygromycin (20 mg/L) for additional two weeks before being subjected to polymerase chain reaction (PCR) to detect 5′ and 3′ homologous recombination.

Agrobacterium-mediated transformation

Multiple moss lines were generated using Agrobacterium-mediated transformation protocol described in NIBB Phycobase resource (<https://moss.nibb.ac.jp/>) with slight modifications. Briefly, *Agrobacterium tumefaciens* (strain GV2260) harbouring pCAMBIA1300-SCR1:GUS-NosT vector grown in 5 ml of LB/Kanamycin media for 48 h at 30 °C and co-cultured with 4 days old wild type (WT) *P. patens* protonema. After 2 days, co-cultured protonemal tissues were transferred to selection media (BCDAT

media supplemented with 50 µg/mL augmentin and 20 µg/mL hygromycin). Surviving tissues through first selection were transferred to relaxation media (BCDAT media supplemented with 50 µg/mL augmentin) and grown for a week and transferred to second selection media (BCDAT media supplemented with 50 µg/mL augmentin and 20 µg/mL hygromycin) for 2 weeks. Surviving lines were selected for GUS staining and histochemical analysis.

RT-qPCR analysis

Total RNA was extracted from 100 mg of three-week old protonema and gametophore tissue, harvested from BCDAT media. Frozen tissue was grounded using a mortar and pestle and RNA was isolated using RNAiso-Plus for RT-qPCR analysis. (Takara Bio USA Inc., CA, USA). Two micrograms of RNA samples were reverse-transcribed using oligo dT primers and SS-IV reverse transcriptase (Invitrogen, CA, USA). Specific PCR primers were designed to detect endogenous *β-actin* (Act_F, Act_R) and ubiquitin-conjugating enzyme E2 (E2 F, E2 R), *PpSCR1* (PpSCR1_qF, PpSCR1_qR), *PpSCR2* (PpSCR2_qF, PpSCR2_qR), and *PpSCR3* (PpSCR3_qF, PpSCR3_qR) transcripts (Supplementary Table S1). cDNA was diluted to 1:10 concentration and relative quantification was performed using the Bio-Rad CFX96 Touch Real-Time PCR Detection System (Bio-Rad, CA, USA). Cyclor conditions were as follows 95 °C for 10 s; 40 cycles of 95 °C for 5 s and 55 °C for 30 s, and an additional step for melting curve analysis at 95 °C for 10 s. SYBR green used for detection of transcripts was SYBR Premix Ex Taq II (Tli RNaseH Plus) from Takara (Takara Bio USA Inc., USA). Each plate was run with samples including no cDNA template control. Relative target gene expression levels were carried out using *β-actin* and ubiquitin-conjugating enzyme E2 as a reference genes, whose expression is stable (Supplementary Table S4) across different growth conditions in moss gametophytes (Le Bail et al. 2013). Fold-change (sample value/reference value) was calculated based on the $2^{-\Delta\Delta C_t}$ method of Schmittgen and Livak (Schmittgen and Livak 2008).

Phenotypic characterization

One month old *P. patens* colonies were used to measure the colony diameter and gametophore height. The 7th–10th leaf from the apex was dissected from one month old gametophores, and the leaf length, width and cell numbers were recorded for n = 20 plants using Olympus stereomicroscope (Olympus, Japan) and ImageJ (Schindelin et al. 2012). To prepare the leaf array silhouettes, the first nine leaves of each transgenic line were imaged using Leica S8 APO Stereo-microscope (Leica Microsystems, Germany) and traced using Inkscape (Version 0.92.3–1).

GUS staining

GUS staining was performed as per protocol of Jefferson et al. 1987 (Jefferson et al. 1987) with minor modifications. Briefly, one month old moss gametophores grown on BCDAT media were fixed in 0.3% formaldehyde solution and incubated at 37 °C for 12 h in GUS solution. After fixation with 5% formalin followed by 5% acetic acid, tissue was dehydrated in a series of ethanol gradients (30%–100%). After the complete removal of chlorophyll contents, gametophore and leaves were visualised and documented using Leica S8 APO Stereo-microscope.

Propidium iodide staining

One-month-old gametophores were submerged in a solution of 20 µg mL⁻¹ propidium iodide (PI) for 10 min, mounted on a slide using a drop of water and imaged using a Leica SP8 confocal microscope with a 40× oil immersion lens. Fluorescence was observed after excitation with a 488 nm Argon laser at 30% laser power and detection within a range of 600–630 nm as per previous protocols (Moody et al. 2021).

Histological analysis

For histology studies, *P. patens* gametophores were fixed in a solution of 10% formaldehyde, 50% ethanol, and 5% acetic acid. Chlorophyll was removed by a series of ethanol washes and was serially replaced with xylene followed by paraffin wax. Thin Sections. (10 µm in thickness) were taken using a Leica RM2265 microtome (Leica Microsystems, Germany). Sections were stained with toluidine blue to increase the visibility of tissue and imaged using a Zeiss Apotome microscope (Carl Zeiss, Bangalore, India). To compare the phenotypes of leaf blade and mid-vein in terms of cell number and area, both WT and mutant leaf sections were analysed. In WT sections, the widest region (oblanceolate shape) was chosen, which lies around two third distance. Since the mutant leaf lacks the typical oblanceolate shape, the sections that lie approximately two third away from the base were used. To calculate the percentages of leaf blade and mid-vein area from the microtome sections, the respective areas were divided by the total area of the corresponding leaf. The area and cell number ratios between leaf blade and mid-vein were also determined for each leaf and subsequently compared between WT and mutant.

Western blot analyses

Three-week-old moss gametophores were crushed in liquid nitrogen and suspended in phosphate buffer saline (PBS) (20 mM, pH 7.4) containing 2X SDS dye and protein extraction was performed (Mohanasundaram et al. 2021). Total

protein from WT, 35S: eGFP and SCR1_OE lines were probed using polyclonal anti-GFP antibody (Cloud clone corp., TX, USA) at a dilution of 1:500 and goat anti-rabbit secondary antibody at a dilution of 1:10,000.

RNAseq analysis

Three-week-old moss colonies of WT and *ppscr1*#12 were grown under a 16:8 light and dark regime at 24°C. Under the stereo-microscope, 100 mg gametophore tissue was harvested in three bio-replicates and frozen immediately. The tissue was ground using pestle and mortar for total RNA isolation using RNAiso Plus (DSS Takara, New Delhi, India). Three µg of total RNA were used to generate sequencing libraries using NEBNext Ultra RNA Library Prep Kit for Illumina (New England Biolabs, MA, USA), following which index codes were assigned to each sample. The library quality was assessed using a Bioanalyzer 2100 system (Agilent Technologies, CA, USA). The clustering of the indexed samples was performed on a cBot Cluster Generation System using a TruSeq PE Cluster Kit v3-cBot-HS (Illumina, CA, USA). After cluster generation, the library preparations were sequenced on an Illumina HiSeq platform, and 150-bp paired-end reads were generated. FastQC analysis was performed on the raw reads to estimate the quality of the data. PCA analysis was carried out in R (Version 1.1.463) to assess the closeness of each replicate to one another. The raw reads were then normalised, indexed and mapped onto the reference *P. patens* genome version 3 (Lang et al. 2018) using the mapping mode of Salmon software (Patro et al. 2017). Differentially expressed genes (DEGs) were uncovered using the DESeq2 package in R (Version 1.1.463). Gene ontology was performed using the Bingo plugin of Cytoscape v3.4.0 by setting the q-value to FDR < 0.01 to detect DEGs (Supplementary Fig. S11-S13) (Shannon et al. 2003). Functional validation of a few selected differentially expressed target genes was done using RT-qPCR. The list of primers used are provided in Supplementary Table S1.

Results

PpSCRs are land plant-specific, GRAS domain containing genes

SCARECROW (SCR) proteins contain GRAS domain towards their C-terminal end. Our homology search analysis using the GRAS domain profile-HMM identified several GRAS domain containing proteins in land plant genomes. However, among streptophycean algae, GRAS domain genes were found only in Zygnematophyceae (sporadically) and were absent in the genomes of *Chara braunii* and *Klebsorbidium nitens*. In addition, chlorophyceae and other distantly

related algal genomes from brown and red algae groups did not have GRAS domain containing proteins (Supplementary Table S2). These results suggested that SCR genes are land plant-specific. To understand the origin of GRAS domain containing proteins and identify its subclades, a maximum likelihood phylogenetic analysis was performed. We identified various clades, such as SCARECROW, SHORTROOT, DELLA, and PAT1. The GRAS domain genes identified from streptophycean algae formed a separate clade, suggesting that the GRAS domain proteins have diverged into different clades in land plants (Fig. 1A, Supplementary Fig. S1). We also identified three SCR homologs in *P. patens* genome (*PpSCR1* – Pp3c19_18560V3.1; *PpSCR2* – Pp3c21_17650V3.1; *PpSCR3* – Pp3c22_13060V3.1). Multiple sequence analysis showed that *P. patens* SCR homologs have all the conserved motifs previously defined in *AtSCR* (Fig. 1B). Intron, exon, and domain organisation arrangement revealed lack of conserved introns among SCR homologs (Fig. 1C). However, the characteristic C-terminal GRAS domain arrangement remains conserved.

PpSCR1 knockout lines exhibited slender leaf phenotype

Knockout studies using stable transgenic lines of the three SCR paralogs revealed that only the *ppscr1* lines showed a distinct slender leaf phenotype (Fig. 2, Supplementary Fig. S2), while *ppscr2* and *ppscr3* lines resembled WT (Supplementary Fig. S3 and S4). Coincidentally, among the three SCR paralogs, *PpSCR1* had the highest expression in WT leaves and gametophores (Fig. 2P). Hence, we focused on *PpSCR1* to study its role in moss development. The knockout lines of *PpSCR1* showed slender leaf phenotype, which was clearly visible in the leaves of a three-week old gametophore (Fig. 2A-N). The overall leaf dimensions appeared to be greatly reduced in the mutant (Fig. 2C – E and H – J, Supplementary Fig. S5). The reduced leaf length and width of *ppscr1* (Fig. 2K and L) was due to the reduced cell numbers at the proximo-distal and medio-lateral axes, respectively (Fig. 2M and N). As nitrogen availability and cytokinin supplementation are both known to regulate moss leaf size (Barker and Ashton 2013), both WT and *ppscr1* were grown in low nitrogen media containing 1 mM nitrate and supplemented with 1 µM BAP (6-Benzylaminopurine), a cytokinin, or without BAP, serving as a control, in BCDAT media (mock). WT gametophores grown in both nitrogen deficient and cytokinin supplemented media exhibited increased leaf width as compared to the control. Though only a small increase in leaf width was observed in the *ppscr1*, it is, however, statistically significant (Fig. 2O). In addition, 1 µM BAP supplementation also induced the *PpSCR1* expression in WT (Supplementary Fig. S6).

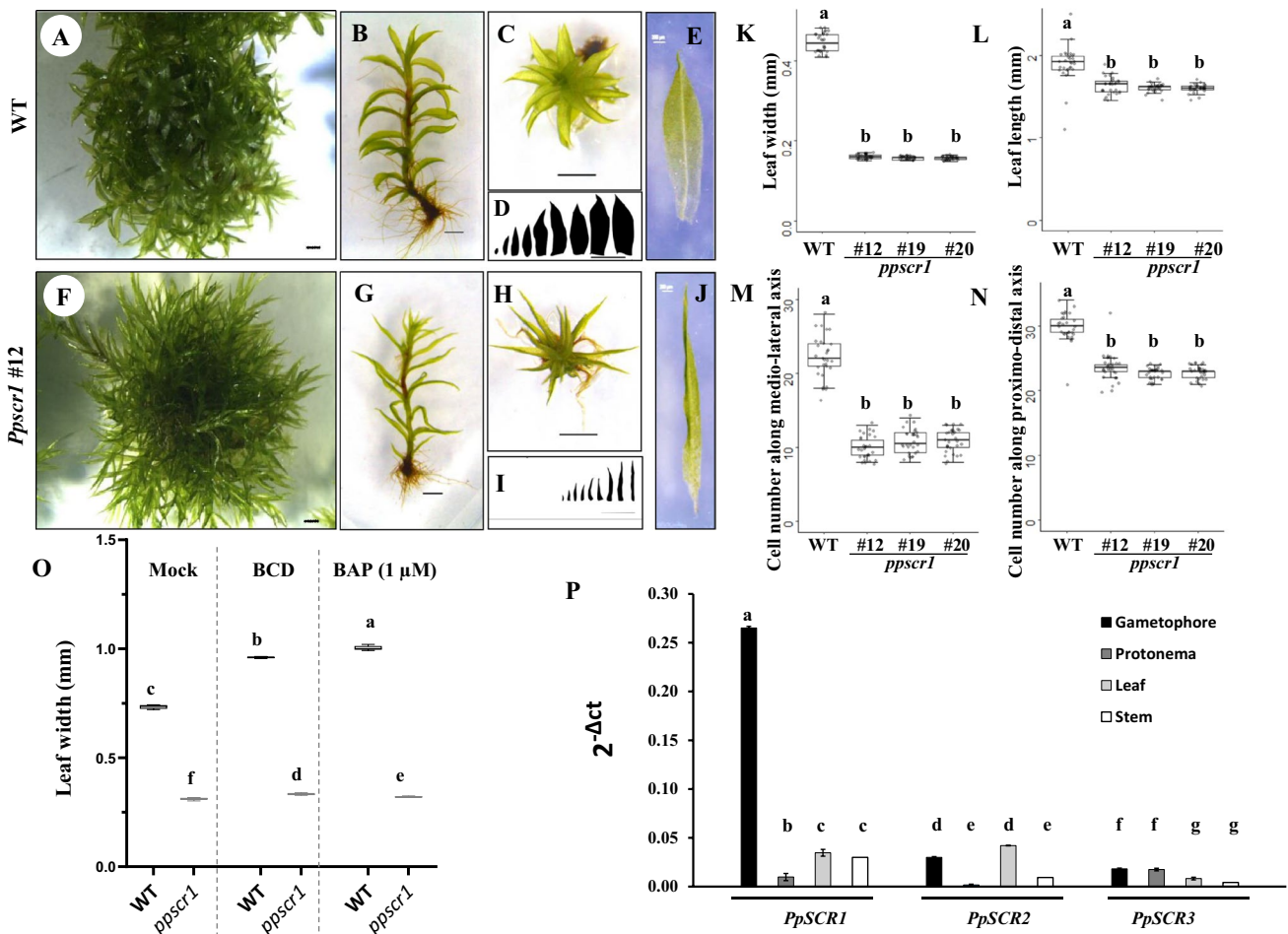


Fig. 2 *PpSCR1* knockout line develops slender leaves due to reduced cell number along the medio-lateral axis. **A–H** One month-old WT (A–E) and *ppscr1* (F–J) colonies, gametophore (side and top view), leaf silhouette and 9th leaf were shown. Scale bar for A–D and F–I is 1 mm, and for E and J is 20 μm. Leaf width (**K**), length (**L**), and cell number along the medio-lateral (**M**) and proximo-distal (**N**) axes of WT and *ppscr1* knockout lines (#12, #19, and #20) are compared

(n=30). **O** The leaf width of WT and *ppscr1*#12 were compared on growth conditions such as BCDAT (mock) and BCD media with and without BAP (1 μM) supplement (n=30). The ANOVA letters above each box indicate the differences between each data set. **P** Tissue-specific expression of *P. patens SCR* homologs was quantified. All statistical analyses were conducted using ANOVA. Bars that do not share a similar letter are significantly different from each other

width of the leaf. These leaf anatomical sections suggested that the differences in cell division pattern possibly caused the slender leaf phenotype.

Altered cell division pattern is the underlying cause of slender leaf phenotype

Previous studies have shown that the leaf apical cell undergoes a series of asymmetric divisions to form different sectors of a leaf primordium (Harrison et al. 2009). These daughter cells further divide to form the leaf blade cells. These developmental steps indicate that mid-vein development occurs later and presumably through further differentiation of leaf blade cells. In *P. patens*, leaf blade cells are large and uni-layered, while the mid-vein cells are

multi-layered and vary in size. To understand the cell division pattern of leaf blade and mid-vein in WT, we analysed a series of transverse microtome sections from the leaf tip to its base. Only leaf blade cells were observed at the leaf tip, as mid-vein was absent at the tip of the *P. patens* leaf (Fig. 4A). Further sections towards the leaf base showed an increase in the number of leaf blade cells and the appearance of mid-vein. The cell 0 denotes the leaf blade cells in the medial cell file of the section (Fig. 4B) that is replaced by mid-vein in the subsequent sections, as evident from the appearance of three layers of cells replacing the medial cell (cell 0) (Fig. 4B–E). Amongst the three layers, the cell files on the adaxial and abaxial side may have divided anticlinally, while the medial cell underwent several anticlinal and periclinal divisions (Fig. 4F–I). At the midrib, a new cell

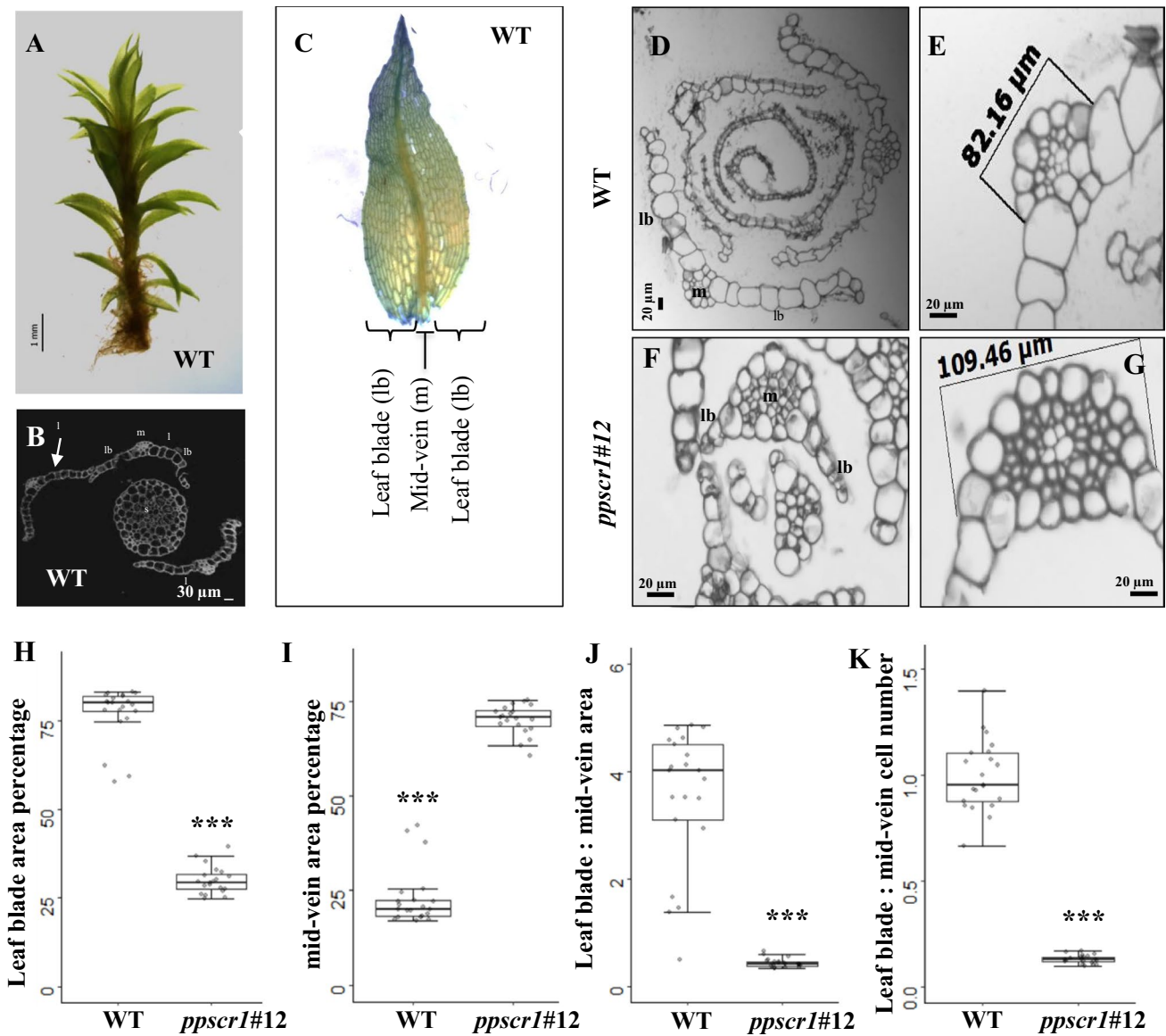


Fig. 3 Anatomical differences in the leaf blade and mid-vein of WT and *ppschr1*. Transverse section of WT gametophore (A) showing the leaf and stem cellular organisation (B). WT leaf showing the leaf blade (lb) and mid-vein (m) (C). Transverse sections of WT (D, E) and *ppschr1#12* (F, G) gametophores showing increased mid-vein area in the mutant. (H–I) Measurement of leaf blade and mid-vein area in

leaf transverse sections of WT and mutant were compared (n=21) (J, K). Ratios between the area of leaf blade and mid-vein area and the number of cells in leaf blade and mid-vein were analysed (n=21). Statistical analyses were performed with Student's t-test. *** marks p-value less than 0.001

emerged through an asymmetric anticlinal division of the leaf blade cell L1, resulting in a smaller daughter cell close to the mid-vein and a larger daughter cell near the leaf blade cells. This observation suggests an asymmetrical division pattern in L1 cells near the mid-vein or an indication of cell division activity within mid-vein. In the next series of sections, the daughter cell file appeared to have divided further and became indistinguishable from the rest of the mid-vein. On the other hand, the larger cell file did not divide and resembled the other leaf blade cells (Fig. 4G–I). This series

of anatomical sections suggest that mid-vein differentiates from the leaf blade cells and undergoes periclinal divisions.

We also analysed the leaf sections of mutant leaves to understand the changes that led to the slender leaf phenotype. Similar to WT, mutant leaf tip sections did not have mid-vein (Fig. 4J). Further sections also showed the appearance of three cell layered mid-vein, which replaced the medial cell 0 (Fig. 4H–L). Similar cell division pattern was observed in the mid-veins of three other independent leaf series (Supplementary Fig. S8). In addition, periclinal

WT:

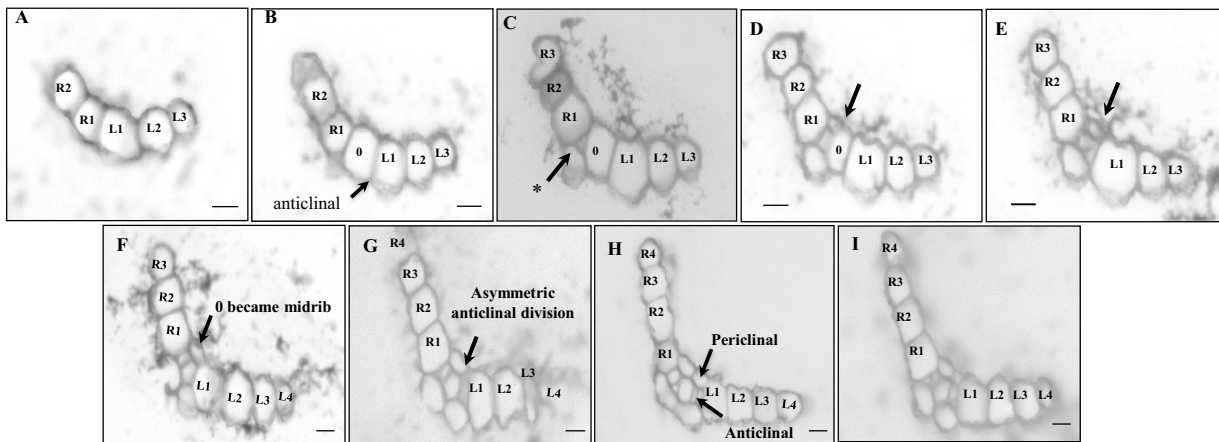
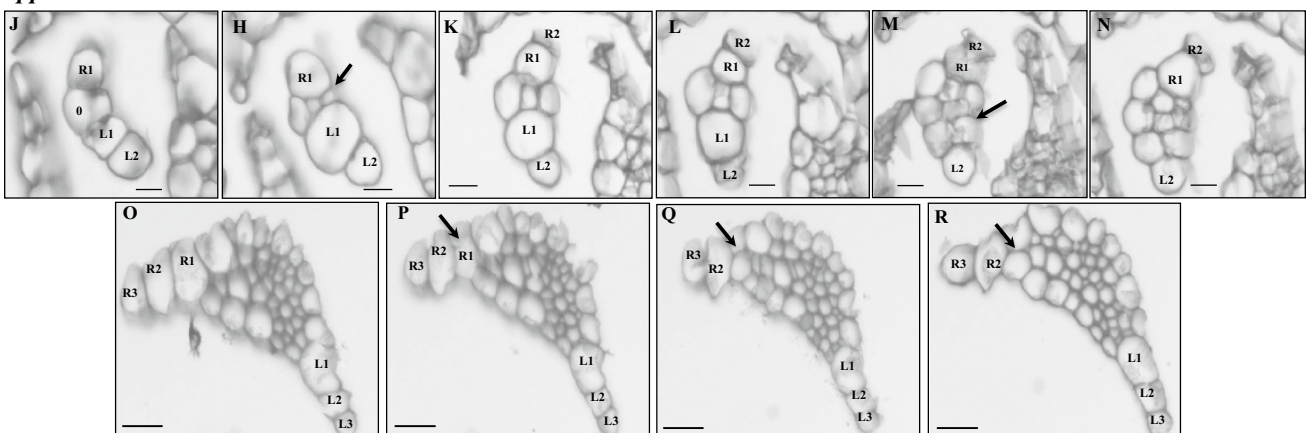
*ppscr1* #12:

Fig. 4 Serial cross section of a wild-type leaf from leaf tip to base. Series cross sections of WT leaf (A–I) and *ppscr1*#12 (J–N and O–R). Leaf blade cells are arbitrarily marked as left (L1, L2, etc.) and right (R1, R2, etc.) leaf blade cells. At the leaf tip, the medial cell file that becomes mid-vein is marked as “0”. **A** At the tip of the WT leaf, mid-vein has not developed yet. The anticlinal division of (**B** and **G**) first leaf blade cell file (L1) leads to the increase in leaf blade width. Also, controlled anticlinal and periclinal divisions (**D**, **E** and **H**) contribute to the mid-vein development. Asterisk in (**C**) marks

sudden increment in cell layer number. Arrow marks cell walls that may have occurred due to asymmetric anticlinal division (**G**). Similarly, *ppscr1*#12 leaf cross section from the tip of the leaf (**J–N**) and from the middle of the proximo-distal axis (**O–R**) is shown. (**H**, **M**) Arrows indicate successive periclinal and anticlinal divisions that lead to the formation of multicellular mid-vein. (**P–R**) Arrows trace the unexpected periclinal division of entire leaf blade cell file R1. Scale = 20 μ m

division was absent in the leaf blade of wild type leaves (Fig. 4, Supplementary Fig. S8). In contrast to the WT pattern, the L1 cell file had undergone multiple divisions and had become a part of the multicellular mid-vein (Fig. 4M, N). Another series of leaf sections towards the middle of the proximo-distal axis suggest that the R1 cell file may have undergone a periclinal division (Fig. 4O–R). Further sections show that the entire R1 cell file became indistinguishable from the rest of the mid-vein. Additional series of sections from leaves show similar periclinal divisions in the leaf blade cells close to the mid-vein (Supplementary Fig. S9). This will lead to the increase in mid-vein cell number and size at the cost of a leaf blade cell and explains the anatomical basis for the larger mid-veins observed in slender

leaf. In addition, we also did not observe any anticlinal division in the leaf blade to increase the width of leaf blade. Hence, we interpret that altered periclinal and anticlinal divisions in leaf blade cells are the cause of slender leaf phenotype in *ppscr1*.

To investigate the tissue-specific activity of *PpSCR1* promoter, *GUS* reporter gene was fused downstream of the *PpSCR1* promoter and two independent lines (*PpSCR1*pro:*GUS*_1 and *PpSCR1*pro:*GUS*_2) generated in WT background were selected for analysis. These transgenic lines did not exhibit any obviously visible phenotypic deviations. WT colony was used as a control where no *GUS* activity was observed (Fig. 5A–D). The *PpSCR1* promoter reporter lines showed intense *GUS* activity in the stem and

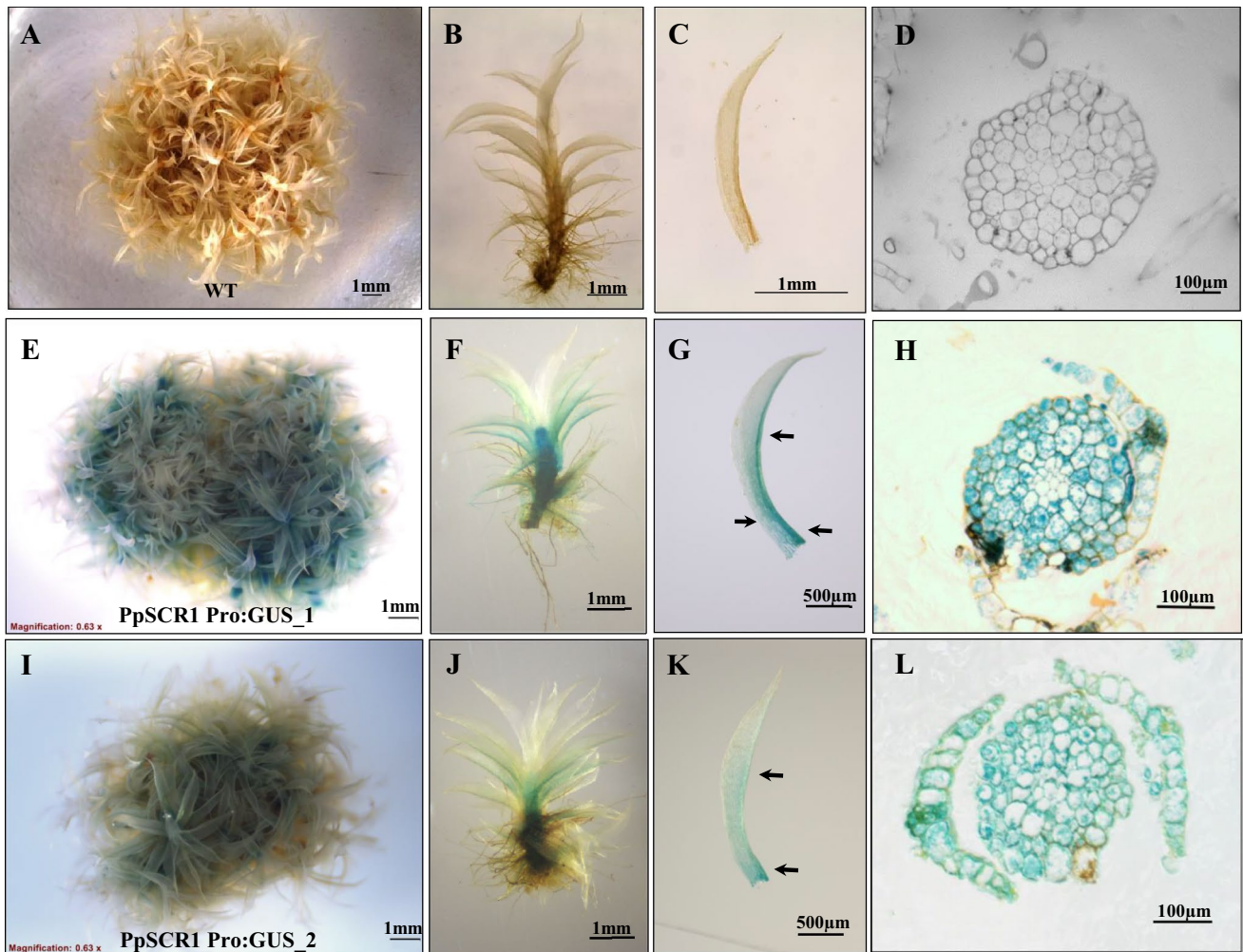


Fig. 5 *PpSCR1* promoter activity in *Physcomitrium patens* gametophore. Two *PpSCR1* promoter lines (*PpSCR1*Pro:GUS #1 and #2) showing GUS expression in colony (A, E, I), gametophore (B, F,

J), and leaf (C, G, K). Cross sections through stem and leaves reveal intense GUS staining in mid-vein, epidermis and cortex (D, H)

mid-vein of leaves and a mild activity along the base of the leaves (Fig. 5 E, F, I, and J). Stem cross sections showed ubiquitous GUS activity in the stem, whereas in leaves, it was prominent in mid-vein compared to the leaf blade (Fig. 5G, H, K, and L). GUS activity was not detected in rhizoids.

PpSCR1 overexpression lines exhibited wider leaves.

We also used a gain of function approach to further understand the function of *PpSCR1*. Though the overexpression construct had GFP fusion, we could not detect GFP fluorescence in the *PpSCR1* OE lines. Despite significant overexpression of SCR1 and formation of GFP transcripts in these lines (Fig. 6E-F), western blot analyses with anti-GFP did not show SCR1-GFP fusion but free GFP protein was detected (Supplementary Fig S10). The *PpSCR1*

overexpression (OE) lines (*PpSCR1* OE#1 and #2) showed morphological differences in the gametophores: the OE lines had significantly broader leaf blades as compared to WT (Fig. 6 A-D). In the *PpSCR1* OE#1 line, the cell number at the medio-lateral axis was significantly higher than WT. Although the cell number at the proximo-distal axes was decreased in the transgenic lines, no difference was observed in the leaf length (Fig. 6C-D). These results suggest that overexpression of *PpSCR1* has impacted the leaf dimensions compared to WT.

Transcriptome analysis of *ppscr1*

To understand gene regulation further, we performed transcriptome analysis on the knockout lines of *PpSCR1* (Supplementary Fig. S11). As a quality control step, the degree of similarity between each bio-replicate was assessed using PCA

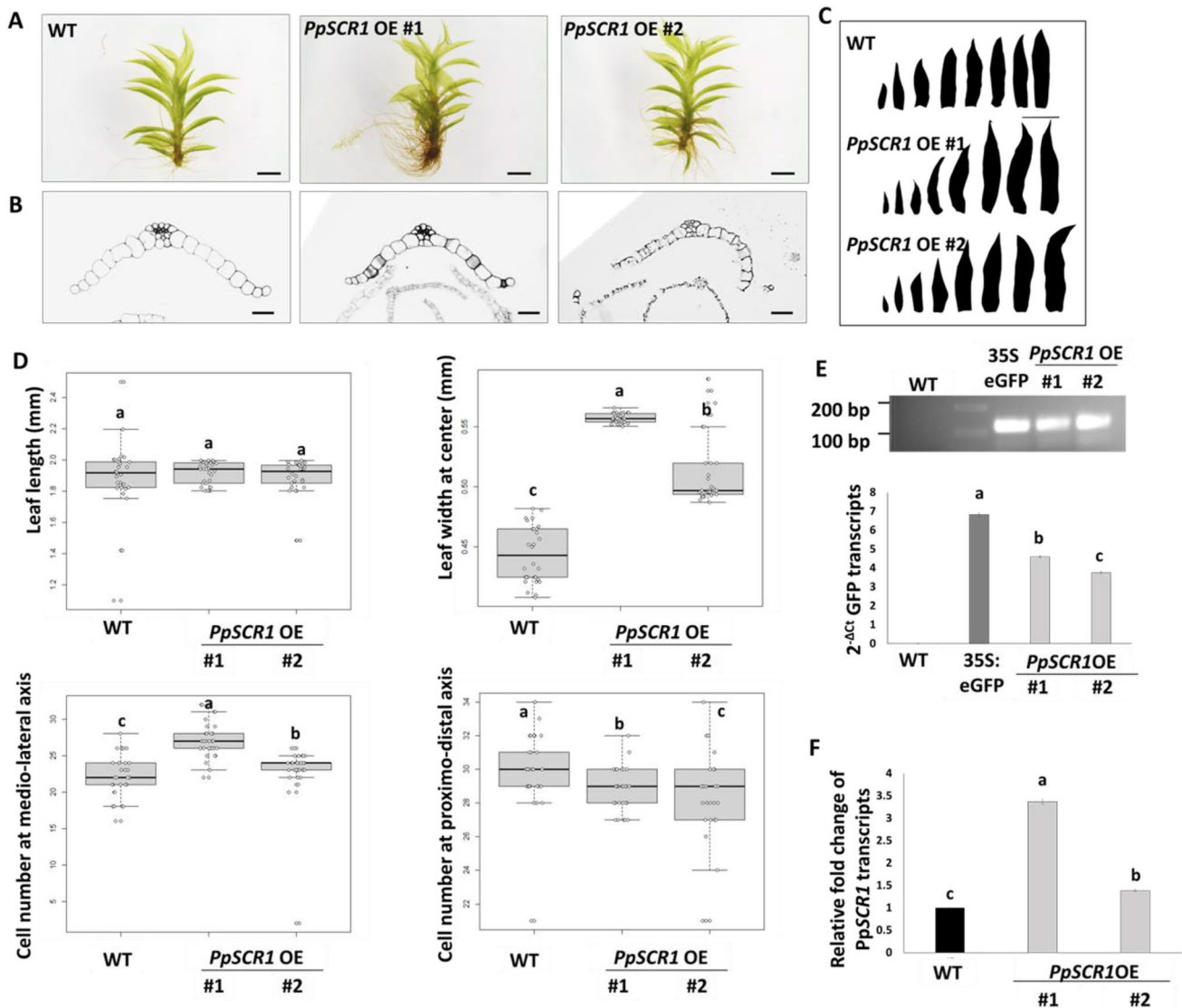


Fig. 6 PpSCR1 overexpression lines displayed broader leaves due to increased cell number at the medio-lateral axis. **A** One-month old gametophores of WT and SCR1 overexpression lines; PpSCR1 OE#1 and #2. **B** Representative leaf cross sections and **C** silhouettes of WT and PpSCR1 OE lines. The scale bar is 50 μ m. **D** Boxplots showing comparative measurements of leaf length and width, and cell

numbers along the proximo-distal and medio-lateral axis of WT and PpSCR1 OE lines ($n=30$). **E** and **F** Graphs showing increased transcript abundance of PpSCR1 in PpSCR1 OE lines as validated by (**E**) eGFP and **F** PpSCR1-specific RT-qPCR ($n=3$). All statistical analyses were conducted using ANOVA. Bars that do not share a similar letter are significantly different from each other

analysis and plotted using scree plots (R Core Team 2021) (Supplementary Fig. S12). A \log_2 fold cut off (± 0.58) was applied to find 5544 differentially regulated genes out of which 3006 and 2538 were up- and down-regulated, respectively, in *ppscr1*. Applying an adjusted p-value of < 0.01 gave 624 and 436 up- and down-regulated genes, respectively (Fig. 7A, B). Word clouds generated using R gives a visual representation of the highest up- and down-regulated genes in *ppscr1*, which were also validated by RT-qPCR (Supplementary Table S3; Fig. 7C-E). Using GO analysis, differentially expressed genes were classified, according to their cellular component, molecular function, and biological processes (Supplementary Fig.

S13-S15). Interestingly, genes regulating biological processes, such as cell division, cell growth and leaf development, cell cycle and cellular organization were found among the differentially expressed genes, though these GO terms are not the most abundant (Supplementary Fig. S15). Callose synthase (Pp3c9_4140 and Pp3c9_4143), Zinc finger domain containing proteins members (Pp3c5_2897, Pp3c6_26100, Pp3c5_2897, Pp3c16_11700, Pp3c16_11705), auxin efflux carriers (Pp3c10_24880), cellulose synthase (Pp3c6_4064 and Pp3c2_1330), glucan synthase (Pp3c20_20530 and Pp3c24_1607), THIOREDOXIN-LIKE PROTEIN 4B (Pp3c22_7790) were found to be down-regulated in *ppscr1*

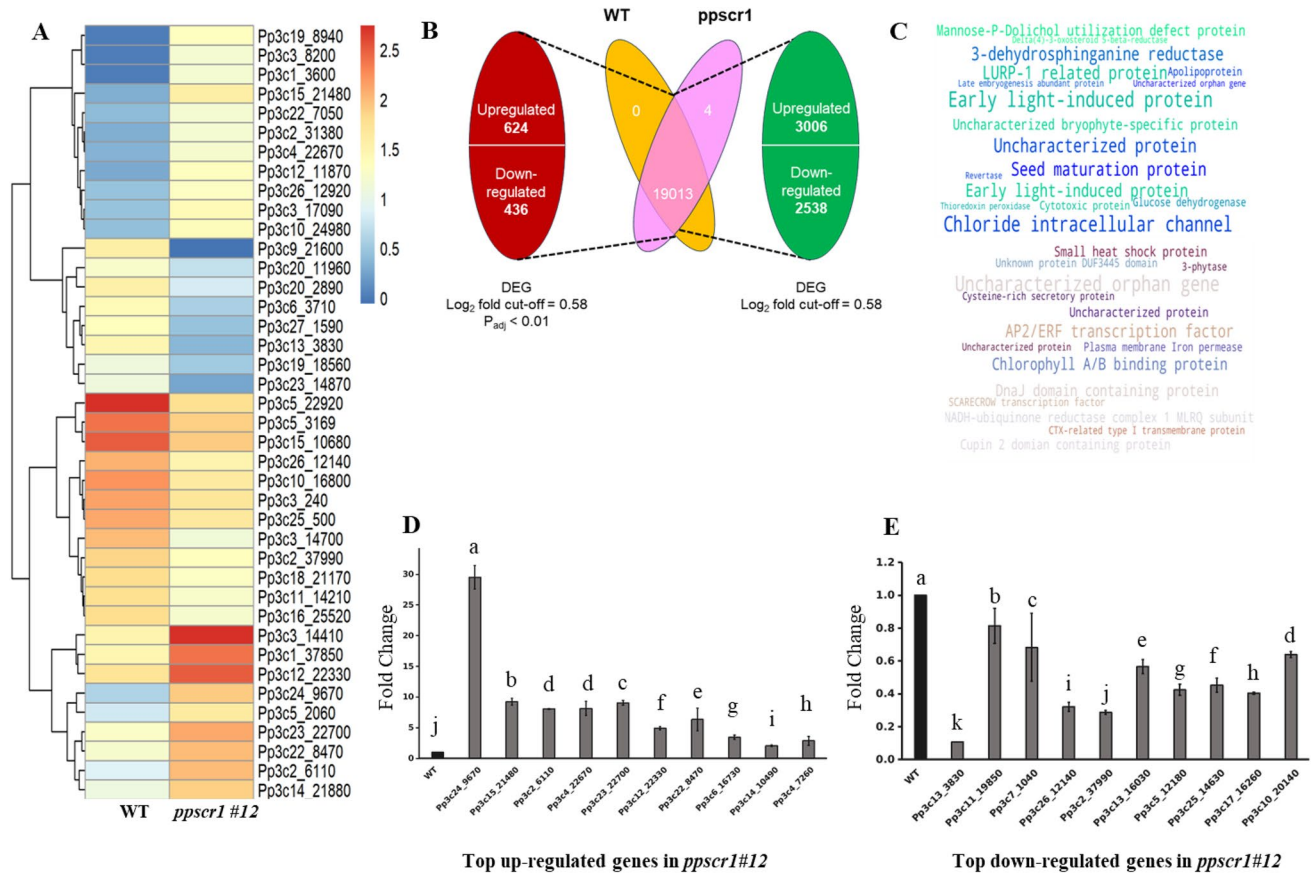


Fig. 7 RNA-Seq analysis of WT and *ppscr1*#12. **A** Hierarchical clustering analysis of top 20 up/down-regulated genes displayed in the form of a heatmap where red and blue colours depict up- and down-regulated genes, respectively. **B** Representation of differentially expressed genes with numbers denoting up/down-regulated genes and those expressing in common and exclusively in WT and *ppscr1*#12. **C** Word cloud representation of top 20 differentially expressed genes

in *ppscr1*#12 where word size corresponds to Log₂ changes in transcript abundance (\log_2 fold change $\frac{\text{mutant}}{\text{wild type}}$). Word clouds have been generated using python (**D–E**). RT-qPCR based validation of the top (**D**) up- and (**E**) down-regulated genes in *ppscr1*#12 transcriptome (n=3). All statistical analyses were conducted using ANOVA. Bars that do not share a similar letter are significantly different from each other

(Supplementary Table S3). BEACH domain containing genes (Pp3c5_2890), MULTIPOLAR SPINDLE 1 (Pp3c7_6690), Rad21/Rec8-like protein, C-terminal, eukaryotic DNA TOPOISOMERASE 3-ALPHA (Pp3c3_26738), MICROTUBULE ASSOCIATED PROTEIN (Pp3c21_9710) and XMAP216 (Pp3c9_24390) were among the up-regulated genes in the mutant (Supplementary Table S3). However, the genes involved in the regulation of cell cycle phase transition, including Cyclin-Dependent Kinases (CDKA; CDKB), Cell Division Cycle proteins (CDCB; CDCD) and Retinoblastoma-Related (RBR), were not differentially expressed in the mutant.

Discussion

The molecular function of SCARECROW (SCR), a GRAS domain transcription factor, has been well-studied for root and leaf development in flowering plants. At the time we

initiated our study, there was no literature that described the function of GRAS domain containing proteins in moss. Very recently, Ge et al., and Ishikawa et al., have demonstrated the role of PpLAS (LATERAL SUPPRESSOR) and PpSHR (SHORT-ROOT) in moss leaf mid-vein development, respectively (Ge et al. 2022; Ishikawa et al. 2023). In the latter study, through knockout and cell segmentation image analyses, authors reported that PpSCR1 and PpLAS have positive and negative regulatory effects on PpSHR, respectively. However, this study was limited to leaf primordium analysis. In our current investigation, through a comprehensive approach, we describe the cellular and molecular basis of the *ppscr1* slender leaf phenotype. Our results show that PpSCR1, a member of SCARECROW clade, governs leaf shape in moss by regulating cell division planes and proliferation.

PpSCR1 is involved in leaf blade and mid-vein development in moss

Mosses have diverse leaf shapes, such as oblanceolate (*Physcomitrium patens*), slender leaf (*Bartramia pomiformis*, *Dicranum scoparium*, *Pleuridium subulatum*), leaves with mid-vein protruding outside the leaf blade (*Phascum cuspidatum*), and leaves with no mid-vein (*Sphagnum fallax*) (Eckel 2004) etc. Notably, in the *ppscr1* mutant, the *P. patens* leaf shape changed from oblanceolate to slender-type (Fig. 2). Additionally, we observed that the *ppscr1* mutant was less sensitive to both nitrogen availability and cytokinin supplementation (Fig. 2O), the two factors known to enhance the leaf width of *P. patens* (Barker and Ashton 2013). This suggests that these factors may function upstream of *PpSCR1* gene. In line with this hypothesis, *PpSCR1* expression was enhanced in WT tissue upon cytokinin supplementation (Supplementary Fig. S6).

In a previous study, Harrison et al., (2009) performed X-ray irradiation on chloroplast biogenesis mutant to show that moss leaves contain up to 17 segments or merophytes, which are daughter cells formed by successive asymmetric divisions from the leaf apical cell. Further, by using live microscopy, they showed that initial cell divisions inside a segment are longitudinal, which leads to an increased number of cells (anticlinal) along the medio-lateral axis, expanding the leaf width. We speculate that *ppscr1* slender leaves are caused either by impaired anticlinal cell divisions or uninhibited periclinal divisions. Harrison et al., (2009) also showed that successive cell divisions in the primordium are along the proximo-distal axis, which is reminiscent of cell files observed in monocot leaves; however, moss leaf cell files are discontinuous and limited to their segments. Our histological analysis suggests that the WT moss leaf blade cell files flanking the mid-vein may undergo an asymmetric anticlinal division, and the smaller daughter cell file becomes a part of mid-vein, while the larger cell file remains as a leaf blade cell. Alternatively, mid-vein cell division could be the source of the new cell (Fig. 4 and Supplementary Fig. S16). In *ppscr1* mutant, the leaf blade cell flanking the mid-vein would divide periclinally and integrate into the mid-vein (Fig. 4, Supplementary Fig. S9). In line with our histology observations, *PpSCR1* promoter activity was also detected throughout the main stem and leaf; however, it was more intense at the mid-vein (Fig. 5). RT-qPCR analysis showed high expression of *PpSCR1* only in leaf and stem but not in the protonema (Fig. 2P). Accordingly, we did not find any visible difference in protonema development of *ppscr1*. Recently, *PpSCR1* mRNA has also been proposed as a marker for bud formation and gametophore initiation (Moody et al. 2021). All these results suggest that the *PpSCR1* is an important factor controlling cell division

planes to regulate leaf blade and mid-vein development in moss.

SCARECROW plays a conserved role in regulation of cell division

GRAS domain containing proteins are plant-specific, and they are found in all land plants and Zygnematophyceae but not among other charophycean algae, such as *Chara braunii* and *Klebsormidium nitens* (Supplementary Table S2). GRAS domain containing genes in flowering plants have been classified into eight different clades (Bolle 2004; Tian et al. 2004). By including the GRAS domain containing proteins of *Selaginella moellendorffii* and *Physcomitrium patens* and few coding sequences (CDS) from the charophycean algae *Spirogyra* (Zygnematophyceae class), Engstrom et al., (2011) expanded this analysis to all land plants, and the authors concluded that these eight different clades have diverged before the origin of land plants. Though this study suggested that GRAS domain containing proteins are ancient, it could not resolve the phylogenetic history amongst charophycean algal members because of the absence of genomic resources at that time. Our analyses included GRAS domain containing proteins from three Zygnematophyceae genomes (*Mesotaenium endlicherianum*, *Spirogloea musicola*, *Penium margaritaceum*). A single clade consisting of most of the Zygnematophyceae proteins formed in the phylogenetic tree, suggesting that the previously identified eight clades, including SCR clade, are land plant-specific (Supplementary Fig. S1). Future analyses with more genomic resources could only help to identify the ancestral form of GRAS genes.

Moss leaves share few morphological similarities with flowering plant leaves (megaphylls); the leaf shape and the presence of mid-vein are comparable features. Our results suggest that the knockout lines of *PpSCR1* produced leaves with thicker mid-vein because of the periclinal cell division in the leaf blade cells flanking mid-vein. (Fig. 3 and 4, Supplementary Fig. S9). Our findings are consistent with a recent report, wherein the authors describe the role of SHR-SCR module in regulation of cell division in moss leaves (Ishikawa et al. 2023). Similarly, leaves of Arabidopsis *scr* mutant were smaller compared to WT, because of reduced cell division along both proximo-distal and medio-lateral axes. *scr* leaf cells undergo early exit from the cell proliferation phase, causing reduced leaf growth (Dhondt et al. 2010). The maize leaf (megaphyll) is capable of C4 photosynthesis wherein a layer of photosynthetic bundle sheath cells surrounds the leaf vein (Chollet and Ogren 1973). In maize, SCR loss of function mutant leaves showed excess bundle sheath layers (~4 layers), increasing the overall vein diameter. This phenotype can be due to the increased periclinal cell division at the bundle sheath layer

(Slewisinski et al. 2012) and is comparable to the thicker mid-vein of *ppscr1* leaves. Furthermore, this comparison can be expanded to the flowering plant roots as well. The bundle sheath cells of maize leaves are comparable with the endodermis of Arabidopsis root as both layers of cells surround the vascular bundle and function as the starch sheath. The roots of Arabidopsis *scr* mutant have a single, undifferentiated layer in place of distinct endodermis and cortical layers. Loss of asymmetric periclinal division of endodermis-cortex mother cell is the cause for this phenotype (Scheres et al. 1995). These results suggest that the role of SCR in regulating cell fate determining cell divisions is conserved between flowering plants and moss. *SCR* also regulates cell proliferation in *P. patens* and *A. thaliana*. In *P. patens*, mature leaves obtain their characteristic oblanceolate shape because of the increased cell division activity at the middle of the leaf along the medio-lateral axis; as a result, cell number along this axis is maximum at this region (Harrison et al. 2009). In *ppscr1* mutant, a significant reduction in cell number at the middle of leaf blade, along the medio-lateral axis caused the slender leaf phenotype (Fig. 2).

In contrast, PpSCR1 OE lines showed wider leaf lamina than WT (Fig. 6 A-D). These observations further confirm the role of PpSCR1 in controlling leaf shape. Despite several attempts, we could not detect GFP fluorescence signal in the PpSCR1-GFP OE lines, though GFP transcripts and free GFP protein were detected (Fig. 6 E, F and Supplementary Fig. S10), which could be due to the possible cleavage of the C-terminal GFP tag in these lines. The increased leaf width of the overexpression lines suggests a direct correlation between leaf width and *PpSCR1* expression levels. Additionally, our RNAseq analysis of the *ppscr1* showed that the genes responsible for cell division and proliferation, cell growth and leaf development were significantly down-regulated (Supplementary Table S3), suggesting the role of PpSCR1 in regulating leaf shape through cell division. In a previous report of *PpSHR*, the authors hypothesised that, similar to Arabidopsis, all GRAS domain containing proteins in moss may be involved in the regulation of G2/M cell cycle progression (Ishikawa et al. 2023). However, our transcriptome analyses of the *ppscr1* mutant did not reveal differential regulation of cell cycle checkpoint factors, including Retinoblastoma-Related (RBR), Cyclin-Dependent Kinases (CDKA; CDKB) and Cell Division Cycle proteins (CDCB; CDCD). This indicates that PpSCR1 may not be involved in G2/M cell cycle transition. In summary, our results demonstrate that PpSCR1 is indispensable for moss leaf development. Given the functional conservation of SCR in bryophytes and flowering plants, and the fact that it originates before the divergence of vascular and nonvascular plants, we propose that the role of SCR in controlling cell division and cell proliferation is ancestral.

Supplementary Information The online version contains supplementary material available at <https://doi.org/10.1007/s11103-023-01398-6>.

Acknowledgements We thank Prof. Mitsuyasu Hasebe, NIBB, Japan for sharing knockout vectors (pTN182 and pTN186). We sincerely thank Prof. Magdalena Bezanilla, University of Dartmouth, USA, for the kind gift of Gateway vectors. Technical help received from Mr Vyankatesh Rajmane, Ms Sukanya Jogdand, and Ms Arati Vasav is gratefully acknowledged. The present study was supported by a grant (Grant No. EMR/2016/004852) from the Science and Engineering Research Board (SERB), Government of India to AKB. Core funding and infrastructure were provided by the Indian Institute of Science Education and Research (IISER) Pune, India.

Author contributions B.M and A.K.B designed the experiments and wrote the manuscript. B.M and S.P constructed the vectors and generated transgenic lines. B.M and A.J.B performed histological analyses. S.P carried out microscopic and phenotypic analyses, western blotting and transcriptomic data analyses. A.J.B conducted gene expression analyses and SCR promoter line characterization. M.P. generated *PpSCR2* and *PpSCR3* knockout lines. K.R. performed propidium iodide-based staining and image analyses. P.G generated PpSCR1 promoter lines. B.M, S.P, and A.J.B. have contributed to experimental planning, troubleshooting and data interpretation. A.K.B conceived the project, obtained funding and all necessary resources, interpreted data, edited the manuscript, and supervised the entire study. All authors read and approved the final manuscript.

Funding The financial support received from the Science and Engineering Research Board, Government of India, through Grant No. EMR/2016/004852 is gratefully acknowledged.

Data availability Sequence data from this article can be found in the GenBank data libraries under accession number(s) SAMN36465315 (*scr RNA-Seq* Replicate 1), SAMN36465316 (*scr RNA-Seq* Replicate 2), SAMN36465317 (*scr RNA-Seq* Replicate 3), SRR22982408 (WT *RNA-Seq* Replicate 1), SRR22982407 (WT *RNA-Seq* Replicate 2) and SRR22982406 (WT *RNA-Seq* Replicate 3). The data supporting the findings and claims of this study is mentioned in the main text and is available with the corresponding author.

Declarations

Conflict of interest The authors declare that they have no conflicts of interest.

References

- Barker EI, Ashton NW (2013) Heteroblasty in the Moss, *Aphanogma Patens* (*Physcomitrella Patens*), results from progressive modulation of a single fundamental leaf developmental programme. *J Bryol* 35(3):185–196. <https://doi.org/10.1179/1743282013Y.0000000058>
- Benfey PN, Linstead PJ, Roberts K, Schiefelbein JW, Hauser M-T, Aeschbacher RA (1993) Root development in arabidopsis : four mutants with dramatically altered root morphogenesis. *Development* 119(1):57–70. <https://doi.org/10.1242/dev.119.1.57>
- Bolle C (2004) The role of GRAS proteins in plant signal transduction and development. *Planta* 218(5):683–692. <https://doi.org/10.1007/s00425-004-1203-z>
- Capella-Gutiérrez S, Silla-Martínez JM, Gabaldón T (2009) TrimmAl: a tool for automated alignment trimming in large-scale

- phylogenetic analyses. *Bioinformatics* 25(15):1972–1973. <https://doi.org/10.1093/bioinformatics/btp348>
- Chollet R, Ogren WL (1973) Photosynthetic carbon metabolism in isolated maize bundle sheath strands. *Plant Physiol* 51(4):787–792. <https://doi.org/10.1104/pp.51.4.787>
- Clark NM, Fisher AP, Berckmans B, Van den Broeck L, Nelson EC, Nguyen TT, Bustillo-Avenidaño E, Zebell SG, Moreno-Risueno MA, Simon R, Gallagher KL, Sozzani R (2020) Protein complex stoichiometry and expression dynamics of transcription factors modulate stem cell division. *Proc Natl Acad Sci* 117(26):15332–15342. <https://doi.org/10.1073/pnas.2002166117>
- Cove DJ, Perroud P-F, Charron AJ, McDaniel SF, Khandelwal A, Quatrano RS (2009) The moss *Physcomitrella patens*: a novel model system for plant development and genomic studies. *Cold Spring Harb Protoc*. <https://doi.org/10.1101/pdb.emo115>
- De Smet I, Beeckman T (2011) Asymmetric Cell Division in Land Plants and Algae: The Driving Force for Differentiation. *Nat Rev Mol Cell Biol* 12(3):177–188. <https://doi.org/10.1038/nrm3064>
- Dennis RJ, Whitewoods CD, Jill C, Harrison. (2019) Quantitative methods in like-for-like comparative analyses of *Aphanorhagma* (*Physcomitrella*) Patens Phyllid Development. *J Bryol* 41(4):314–321. <https://doi.org/10.1080/03736687.2019.1668109>
- Dhondt S, Coppens F, De Winter F, Swarup K, Merks RMH, Inzé D, Bennett MJ, Beemster GTS (2010) SHORT-ROOT and SCARECROW regulate leaf growth in arabidopsis by stimulating s-phase progression of the cell cycle. *Plant Physiol* 154(3):1183–1195. <https://doi.org/10.1104/pp.110.158857>
- Eckel, P. M. 2004, Preliminary Cryptogamic (Moss, Lichen and Liverwort) Flora of the Canadian and American Gorge at Niagara Falls, *Res Botanica*, a Missouri Botanical Garden Web site, St. Louis, MO 128 pp.
- Engstrom EM (2011) Phylogenetic Analysis of GRAS Proteins from moss, lycophyte and vascular plant lineages reveals That GRAS genes arose and underwent substantial diversification in the ancestral lineage common to bryophytes and vascular plants. *Plant Signal Behav* 6(6):850–854. <https://doi.org/10.4161/psb.6.6.15203>
- Gázquez A, Beemster GTS (2017) What determines organ size differences between species? a meta-analysis of the cellular basis. *New Phytol* 215(1):299–308. <https://doi.org/10.1111/nph.14573>
- Ge Y, Gao Yi, Jiao Y, Wang Y (2022) A conserved module in the formation of moss midribs and seed plant axillary meristems. *Sci Adv*. <https://doi.org/10.1126/sciadv.add7275>
- Harrison CJ, Corley SB, Moylan EC, Alexander DL, Scotland RW, Langdale JA (2005) Independent recruitment of a conserved developmental mechanism during leaf evolution. *Nature* 434(7032):509–514
- Harrison CJ, Roeder AHK, Meyerowitz EM, Langdale JA (2009) Local cues and asymmetric cell divisions underpin body plan transitions in the moss *physcomitrella patens*. *Curr Biol* 19(6):461–471. <https://doi.org/10.1016/j.cub.2009.02.050>
- Higuchi Y, Kawakita A (2019) Leaf shape deters plant processing by an herbivorous weevil. *Nature Plants* 5(9):959–964
- Horiguchi G, Tsukaya H (2011) Organ size regulation in plants: insights from compensation. *Front Plant Sci*. <https://doi.org/10.3389/fpls.2011.00024>
- Ishikawa M, Fujiwara A, Kosetsu K, Horiuchi Y, Kamamoto N, Umakawa N, Tamada Y et al (2023) GRAS transcription factors regulate cell division planes in moss overriding the default rule. *Proc Natl Acad Sci* 120(4):e2210632120
- Jefferson RA, Kavanagh TA, Bevan MW (1987) GUS fusions: beta-glucuronidase as a sensitive and versatile gene fusion marker in higher plants. *EMBO J* 6(13):3901–3907. <https://doi.org/10.1002/j.1460-2075.1987.tb02730.x>
- Kalyanamoorthy S, Minh BQ, Wong TKF, von Haeseler A, Jermiin LS (2017) ModelFinder: fast model selection for accurate phylogenetic estimates. *Nat Methods* 14(6):587–589. <https://doi.org/10.1038/nmeth.4285>
- Katoh K, Standley DM (2013) MAFFT multiple sequence alignment software version 7: improvements in performance and usability. *Mol Biol Evol* 30(4):772–780. <https://doi.org/10.1093/molbev/mst010>
- Lang D, Ullrich KK, Murat F, Fuchs J, Jenkins J, Haas FB, Piednoel M et al (2018) The *Physcomitrella Patens* Chromosome-scale Assembly Reveals Moss Genome Structure and Evolution. *Plant J* 93(3):515–533. <https://doi.org/10.1111/tjp.13801>
- Le Bail A, Scholz S, Kost B (2013) Evaluation of Reference Genes for RT QPCR analyses of structure-specific and hormone regulated gene expression in *physcomitrella patens* Gametophytes. *PLoS ONE* 8(8):e70998
- Leigh A, Sevanto S, Close JD, Nicotra AB (2017) The Influence of Leaf Size and Shape on Leaf Thermal Dynamics: Does Theory Hold up under Natural Conditions? *Plant, Cell Environ* 40(2):237–248
- Lin W, Wang Y, Coudert Y, Kierzkowski D (2021) Leaf Morphogenesis: Insights from the Moss *Physcomitrium Patens*. *Front Plant Sci* 12:736212
- Mohanasundaram B, Bhide AJ, Palit S, Chaturvedi G, Lingwan M, Masakapalli SK, Banerjee AK (2021) The Unique Bryophyte-Specific Repeat-Containing Protein SHORT-LEAF Regulates Gametophore Development in Moss. *Plant Physiol* 187(1):203–217. <https://doi.org/10.1093/plphys/kiab261>
- Moody LA (2022) Unravelling 3D Growth in the Moss *Physcomitrium Patens*. *Essays Biochem* 66(6):769–779
- Moody LA, Kelly S, Clayton R, Weeks Z, Emms DM, Langdale JA (2021) NO GAMETOPHORES 2 Is a Novel Regulator of the 2D to 3D Growth Transition in the Moss *Physcomitrella Patens*. *Curr Biol* 31(3):555–563.e4. <https://doi.org/10.1016/j.cub.2020.10.077>
- Nguyen L-T, Schmidt HA, von Haeseler A, Minh BQ (2015) IQ-TREE: A Fast and Effective Stochastic Algorithm for Estimating Maximum-Likelihood Phylogenies. *Mol Biol Evol* 32(1):268–274. <https://doi.org/10.1093/molbev/msu300>
- Nicotra AB, Andrea Leigh C, Boyce K, Jones CS, Niklas KJ, Royer DL, Tsukaya H (2011) The Evolution and Functional Significance of Leaf Shape in the Angiosperms. *Funct Plant Biol* 38(7):535–552
- Nishiyama T (2000) Tagged Mutagenesis and Gene-Trap in the Moss, *Physcomitrella Patens* by Shuttle Mutagenesis. *DNA Res* 7(1):9–17. <https://doi.org/10.1093/dnares/7.1.9>
- Patro R, Duggal G, Love MI, Irizarry RA, Kingsford C (2017) Salmon Provides Fast and Bias-Aware Quantification of Transcript Expression. *Nat Methods* 14(4):417–419. <https://doi.org/10.1038/nmeth.4197>
- Perilli S, Di Mambro R, Sabatini S (2012) Growth and Development of the Root Apical Meristem. *Curr Opin Plant Biol* 15(1):17–23. <https://doi.org/10.1016/j.pbi.2011.10.006>
- Pysh LD, Wysocka-Diller JW, Camilleri C, Bouchez D, Benfey PN (1999) The GRAS gene family in Arabidopsis: Sequence characterization and basic expression analysis of the SCARECROW-LIKE genes. *Plant J* 18:111–119
- R Core Team (2021) R: A Language and Environment for Statistical Computing. R Foundation for Statistical Computing, Vienna
- Scheres B, Di Laurenzio L, Willemsen V, Hauser M-T, Janmaat K, Weisbeek P, Benfey PN (1995) Mutations Affecting the Radial Organisation of the Arabidopsis Root Display Specific Defects throughout the Embryonic Axis. *Development* 121(1):53–62. <https://doi.org/10.1242/dev.121.1.53>
- Schindelin J, Arganda-Carreras I, Frise E, Kaynig V, Longair M, Pietzsch T, Preibisch S et al (2012) Fiji: An Open-Source Platform for Biological-Image Analysis. *Nat Methods* 9(7):676–682. <https://doi.org/10.1038/nmeth.2019>
- Schmittgen TD, Livak KJ (2008) Analyzing Real-Time PCR Data by the Comparative CT Method. *Nat Protoc* 3(6):1101–1108. <https://doi.org/10.1038/nprot.2008.73>

- Shannon P, Markiel A, Ozier O, Baliga NS, Wang JT, Ramage D, Amin N, Schwikowski B, Ideker T (2003) Cytoscape: A Software Environment for Integrated Models of Biomolecular Interaction Networks. *Genome Res* 13(11):2498–2504. <https://doi.org/10.1101/gr.1239303>
- Slewinski TL, Anderson AA, Zhang C, Turgeon R (2012) Scarecrow Plays a Role in Establishing Kranz Anatomy in Maize Leaves. *Plant Cell Physiol* 53(12):2030–2037. <https://doi.org/10.1093/pcp/pcs147>
- Takenaka A (1994) Effects of Leaf Blade Narrowness and Petiole Length on the Light Capture Efficiency of a Shoot. *Ecol Res* 9:109–114
- Tamang BG, Zhang Y, Zambrano MA, Ainsworth EA (2023) Anatomical Determinants of Gas Exchange and Hydraulics Vary with Leaf Shape in Soybean. *Ann Bot* 131(6):909–920
- Tian C, Wan P, Sun S, Li J, Chen M (2004) Genome-Wide Analysis of the GRAS Gene Family in Rice and Arabidopsis. *Plant Mol Biol* 54(4):519–532. <https://doi.org/10.1023/B:PLAN.0000038256.89809.57>
- Tomescu AMF (2009) Megaphylls, Microphylls and the Evolution of Leaf Development. *Trends Plant Sci* 14(1):5–12
- Xu Bo, Ohtani M, Yamaguchi M, Toyooka K, Wakazaki M, Sato M, Kubo M et al (2014) Contribution of NAC Transcription Factors to Plant Adaptation to Land. *Science* 343(6178):1505–1508. <https://doi.org/10.1126/science.1248417>
- Yip HK, Floyd SK, Sakakibara K, Bowman JL (2016) Class III HD-Zip Activity Coordinates Leaf Development in *Physcomitrella*. *Dev Biol* 419(1):184–197. <https://doi.org/10.1016/j.ydbio.2016.01.012>

Publisher's Note Springer Nature remains neutral with regard to jurisdictional claims in published maps and institutional affiliations.

Springer Nature or its licensor (e.g. a society or other partner) holds exclusive rights to this article under a publishing agreement with the author(s) or other rightsholder(s); author self-archiving of the accepted manuscript version of this article is solely governed by the terms of such publishing agreement and applicable law.